Original Article

CRISPR/Cas9-Targeted Deletion of Methyltransferase-like 3 *(METTL3)* in HepG2 Cells: A Preliminary *In Vitro* Platform Toward Advanced m⁶A-Associated MASLD Models

Faezeh Shafiei[1,2,3], PhD; Negar Azarpira[2,3], MD; Mehdi Dianatpour[4,5], PhD; Neda Kamal[4], PhD; Jafar Fallahi[6], PhD; Seyed Mohammad Gheibihayat[7], PhD; Marzieh Lotfi[1,8], PhD; Maryam Fazelzadeh Haghighi[4], PhD; Ali Dadbinpour[9,10,11], PhD

[1]Department of Molecular Medicine, School of Advanced Medical Technologies, Shahid Sadoughi University of Medical Sciences, Yazd, Iran;
[2]Shiraz Institute for Stem Cell and Regenerative Medicine, Shiraz University of Medical Sciences, Shiraz, Iran;
[3]Transplant Research Center, Shiraz University of Medical Sciences, Shiraz, Iran;
[4]Department of Medical Genetics, School of Medicine, Shiraz University of Medical Sciences, Shiraz, Iran;
[5]Stem Cells Technology Research Center, Shiraz University of Medical Sciences, Shiraz, Iran;
[6]Department of Molecular Medicine, School of Advanced Medical Sciences and Technologies, Shiraz University of Medical Sciences, Shiraz, Iran;
[7]Department of Medical Biotechnology, School of Medicine, Shahid Sadoughi University of Medical Sciences, Yazd, Iran;
[8]Biotechnology Research Center, Yazd Reproductive Sciences Institute, Shahid Sadoughi University of Medical Sciences, Yazd, Iran;
[9]Genetics and Environmental Hazards Research Center, Shahid Sadoughi University of Medical Sciences, Yazd, Iran;
[10]Mother and Newborn Health Research Center, Comprehensive Research Institute for Maternal and Child Health, Shahid Sadoughi University of Medical Sciences, Yazd, Iran;
[11]Department of Medical Genetics, Faculty of Medicine, Shahid Sadoughi University of Medical Sciences, Yazd, Iran

Correspondence:
Ali Dadbinpour, PhD;
Department of Genetics, School of Medicine, Campus of Shahid Sadoughi University of Medical Sciences, Shohadaye Gomnam Blvd., Postal code: 89151-73149, Alim Sq., Yazd, Iran
Tel: +98 35 38203415
Email: dadbin11@gmail.com
Received: 21 February 2026
Revised: 17 May 2026
Accepted: 03 July 2026

What's Known

- Methyltransferase-like 3 *(METTL3)*-mediated m⁶A RNA methylation regulates hepatic metabolic homeostasis and contributes to metabolic dysfunction-associated steatotic liver disease (MASLD) pathogenesis.
- In MASLD, METTL3 has context-, cell type-, and disease stage-dependent pathogenic or protective roles.
- Functional dissection is hindered by incomplete gene disruption and residual activity from alternatively spliced METTL3 isoforms.

What's New

- This study established a dual-sgRNA CRISPR/Cas9 strategy for targeted genomic deletion of *METTL3* in HepG2 cells.
- The resulting edited HepG2 cell population provided a preliminary *in vitro* system for investigating *METTL3*-associated m⁶A regulation in a MASLD-relevant context.

Abstract

Background: Metabolic dysfunction-associated steatotic liver disease (MASLD) has emerged as a major contributor to chronic liver pathology. N⁶-methyladenosine (m⁶A) RNA methylation, catalyzed by methyltransferase-like 3 (METTL3), has been implicated in MASLD in a context- and stage-dependent manner, underscoring the need for genetically defined experimental models. This study aimed to establish a clustered regularly interspaced short palindromic repeats (CRISPR)/CRISPR associated protein 9 (Cas9)-based genome-editing strategy for targeted deletion of *METTL3* in HepG2 cells as a preliminary *in vitro* system to support future investigations of m⁶A-dependent regulatory mechanisms in MASLD.

Methods: A CRISPR/Cas9 approach using two single-guide RNAs (sgRNAs) targeting introns 2 and 10 of *METTL3* was employed to induce large-scale genomic excision. The sgRNAs, cloned into the PX458 vector, were co-transfected into HepG2 cells, followed by fluorescence-activated cell sorting (FACS) enrichment of green fluorescent protein (GFP)-positive cells. Targeted deletion was assessed by gap-polymerase chain reaction (gap-PCR) and Sanger sequencing, and editing efficiency was estimated using tracking of indels by decomposition (TIDE) and CRISPR indel detector (CRISPR-ID) analyses.

Results: Gap-PCR produced an approximately 500 bp amplicon consistent with the predicted *METTL3* deletion. Sanger sequencing confirmed precise excision with a frameshift predicted to disrupt the *METTL3* open reading frame. The TIDE analysis indicated an overall editing efficiency of approximately 34%.

Conclusion: This study demonstrated a CRISPR/Cas9-based strategy for targeted deletion of *METTL3* in HepG2 cells, establishing an initial genetically defined *in vitro* framework that provided a foundation for the future development of m⁶A-associated MASLD model systems.

Please cite this article as: Shafiei F, Azarpira N, Dianatpour M, Kamal N, Fallahi J, Gheibihayat SM, Lotfi M, Fazelzadeh Haghighi M, Dadbinpour A. CRISPR/Cas9-Targeted Deletion of *Methyltransferase-like 3 (METTL3)* in HepG2 Cells: A Preliminary *In Vitro* Platform Toward Advanced m⁶A-Associated MASLD Models. Iran J Med Sci. doi: 10.30476/ijms.2026.110780.4665.

Keywords ● *METTL3* ● Genome engineering ● RNA modification ● Hepatic steatosis

Introduction

Metabolic dysfunction-associated steatotic liver disease (MASLD), previously referred to as nonalcoholic fatty liver disease (NAFLD),

Copyright: ©Iranian Journal of Medical Sciences. This is an open-access article distributed under the terms of the Creative Commons Attribution-NoDerivatives 4.0 International License. This license allows reusers to copy and distribute the material in any medium or format in unadapted form only, and only so long as attribution is given to the creator. The license allows for commercial use.

is a leading cause of chronic liver disease worldwide. Its prevalence is estimated to approach one-third of the adult population.[1, 2] Clinically and histopathologically, MASLD encompasses a progressive spectrum of liver injury, initiating with hepatic lipid accumulation. This process may advance through inflammatory and fibrotic stages and, in a subset of patients, progress to cirrhosis and hepatocellular carcinoma. As a result, it constitutes a substantial source of liver-related morbidity and mortality.[3] MASLD pathogenesis is multifactorial, involving insulin resistance, obesity, dyslipidemia, chronic inflammation, and oxidative stress.[4] However, despite extensive investigation of these metabolic, inflammatory, and fibrotic pathways, the molecular drivers governing MASLD initiation and progression remain incompletely understood. This gap in knowledge continues to constrain the development of effective targeted therapeutic strategies.[5] Beyond transcriptional and post-translational regulation, growing evidence highlights epitranscriptomic mechanisms as critical modulators of hepatic metabolic homeostasis.[6] Since MASLD involves dynamic alterations in lipid metabolism, inflammatory signaling, and cellular stress responses, rapid RNA-level regulation of gene expression becomes particularly relevant. In this context, epitranscriptomic mechanisms might link metabolic stress to coordinated changes in hepatic gene expression. Among the epitranscriptomic modifications implicated in post-transcriptional regulation, N⁶-methyladenosine (m⁶A) is the most common internal modification of mammalian mRNA and regulates RNA splicing, stability, nuclear export, and translation in hepatocytes (figure 1).[7, 8] This modification is deposited by a multicomponent methyltransferase "writer" complex, in which methyltransferase-like3 (METTL3) serves as the core catalytic subunit.[9] Disruption of m⁶A homeostasis has been linked to various metabolic and inflammatory disorders, raising the possibility that METTL3-dependent RNA methylation may also influence biological processes relevant to MASLD.[10]

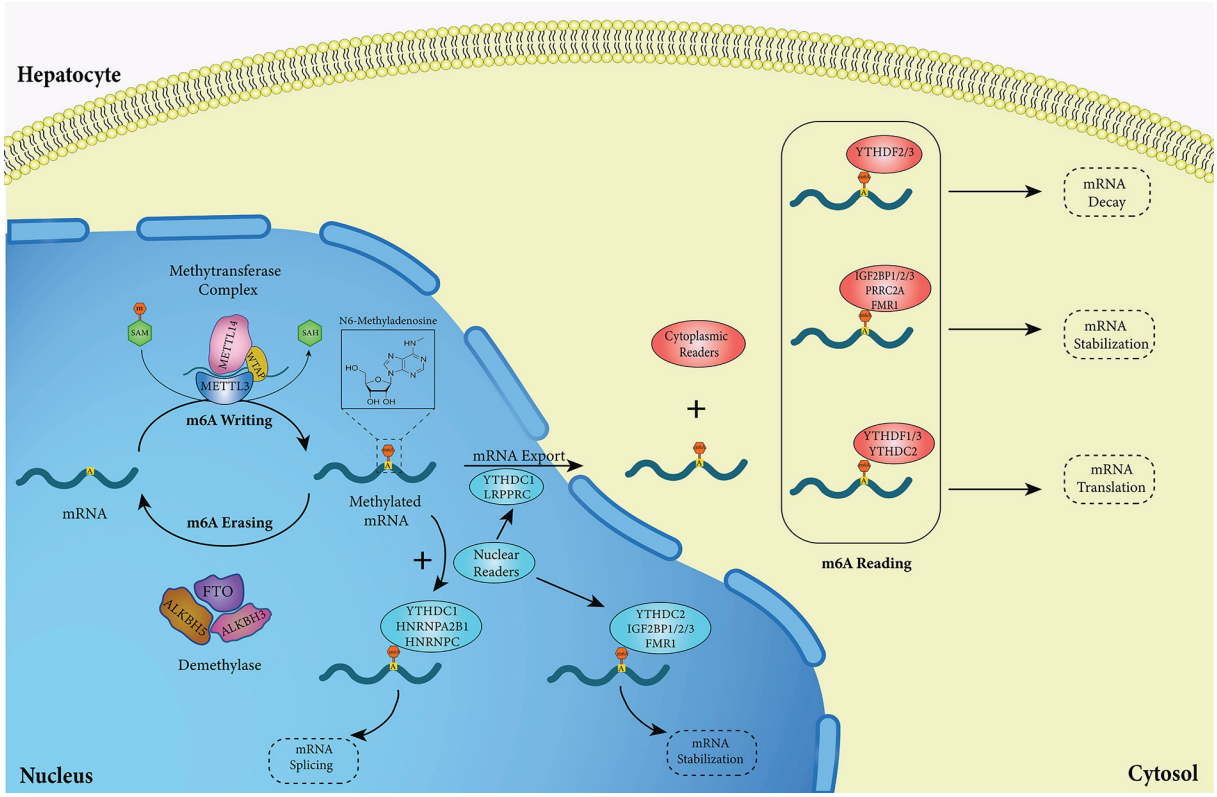


Figure 1: The role of METTL3 within the m⁶A RNA methylation machinery in hepatocytes is illustrated. METTL3, acting as the catalytic core of the writer complex, installs m⁶A marks on RNA transcripts using S-adenosylmethionine (SAM) as the methyl donor, while AlkB homolog 5 (ALKBH5) and fat mass and obesity-associated protein (FTO) serve as erasers to remove these modifications. The m⁶A-marked transcripts are recognized by reader proteins that dictate transcript fate, including mRNA splicing, nuclear export, stability, translation, and decay. Altered m⁶A homeostasis, particularly involving METTL3, has been observed in MASLD. METTL3: methyltransferase-like 3; m⁶A: N⁶-methyladenosine; SAH: S-adenosylhomocysteine; MASLD: Metabolic dysfunction-associated steatotic liver disease MASLD; METTL14: Methyltransferase-like 14; WTAP: Wilms' tumor 1-associating protein; YTHDC1: YTH domain-containing protein 1; YTHDC2: YTH domain-containing protein 2; YTHDF1/2/3: YTH N⁶-methyladenosine RNA binding proteins 1/2/3; IGF2BP1/2/3: Insulin-like growth factor 2 mRNA binding proteins 1/2/3; HNRNPA2B1: Heterogeneous nuclear ribonucleoprotein A2/B1; LRPPRC: Leucine-rich pentatricopeptide repeat-containing protein; FMR1: Fragile X mental retardation protein 1; PRRC2A: Proline-rich coiled-coil protein 2A

However, the functional role of METTL3 in MASLD pathophysiology remains controversial. Multiple studies suggested a pathogenic role for METTL3, showing that its upregulation enhances m⁶A modification of lipogenic and metabolic genes, thereby promoting hepatic lipid accumulation,[7, 11-13] insulin resistance,[14] impaired autophagy,[15] and inflammatory signaling.[13, 14] In contrast, other reports indicated a protective function for METTL3, as hepatocyte-specific deletion exacerbates steatosis, inflammation, and liver injury through dysregulated lipid metabolic gene expression and enhanced fatty acid uptake.[16, 17] Moreover, emerging evidence highlighted cell-type- and stage-specific roles of METTL3 in non-parenchymal liver cells[18-20] and during hepatocarcinogenesis,[21, 22] further underscoring the complexity of its function in MASLD progression.

These discrepancies likely arise from variations in experimental designs, including diverse genetic models, varying dietary regimens, targeting distinct disease stages (e.g., early steatosis versus advanced inflammation), or altering METTL3 expression in specific liver cell populations (e.g., hepatocytes versus immune cells). Collectively, these findings indicated that METTL3 exerted highly context-dependent effects in MASLD, and emphasized the necessity for precise functional dissection using well-defined genetic models.

A key challenge in studying METTL3 function is achieving complete genomic inactivation, as incomplete gene targeting may preserve alternatively spliced isoforms with residual methyltransferase activity, thereby confounding phenotypic interpretation.[23] Moreover, conventional knockdown approaches frequently result in incomplete and transient suppression, limiting their suitability for mechanistic studies.[24,25] To overcome these limitations, precisely engineered Clustered regularly interspaced shortpalindromic repeats/CRISPRassociated protein 9 (CRISPR/Cas9)-based *METTL3* genome-edited systems are required to enable accurate interrogation of m⁶A-dependent mechanisms in MASLD.

The CRISPR-Cas9 system facilitates targeted gene disruption through sgRNA-directed double-stranded DNA cleavage. These lesions are subsequently resolved by error-prone non-homologous end joining (NHEJ) repair machinery, frequently resulting in insertion-deletion mutations.[26] However, single-sgRNA CRISPR approaches frequently generate small indels with heterogeneous functional outcomes and may not reliably disrupt METTL3 catalytic activity.[27, 28] To address this issue, we implemented a dual-single guide RNA (sgRNA) CRISPR/Cas9 strategy[29] targeting intronic regions flanking the *METTL3* locus to induce large-scale genomic excision. This dual-sgRNA design provided a conceptual framework for promoting defined targeted deletion and increasing the likelihood of removing genomic regions corresponding to the catalytic domain.

Materials and Methods

This *in vitro* study was conducted from 2022 to 2025 in the Department of Genetics, School of Medicine, Shiraz University of Medical Sciences, Shiraz, Iran. The study was approved by the Research Ethics Committee of Shahid Sadoughi University of Medical Sciences, Yazd, Iran (Ethics code: IR.SSU.REC.1402.139). All experiments were performed using established human cell lines.

In Silico Design of sgRNAs

Catalytic and functional site annotations of METTL3 were first retrieved from the UniProt Knowledgebase (UniProtKB) (https://www.uniprot.org) to guide the selection of genomic regions for targeted deletion. Using the reference human *METTL3* locus (ENSG00000165819; chr14:21498128–21511362), candidate sgRNAs were designed and systematically evaluated using CRISPOR (http://crispor.tefor.net),[30] Cas-OFFinder (http://www.rgenome.net/cas-offinder/),[31] and CHOPCHOP (https://chopchop.cbu.uib.no/).[32]

Putative sgRNAs were identified based on the presence of suitable protospacer adjacent motif (PAM) sites within intron 2 and the 3′ region of intron 10, flanking the METTL3 catalytic domain. Candidate guides were evaluated using CRISPOR and CHOPCHOP for predicted on-target cleavage efficiency and genome-wide off-target potential. Guides were prioritized based on high predicted on-target efficiency (>60), high specificity (MIT and cutting frequency determination [CFD] scores >90), and minimal predicted off-target sites. The two highest-scoring sgRNAs were selected for experimental validation. Complete sgRNA sequences, primer sets used for detection of the deleted genomic region, and additional design parameters are provided in tables 1 and 2.

This dual-sgRNA strategy was designed to excise the intervening genomic region, with the predicted consequence of altered transcript structure, frameshift formation, and truncation of the catalytic methyltransferase domain.

Table 1: Sequences of the two sgRNAs designed to target introns 2 and 10 of METTL3 for CRISPR/Cas9-mediated targeted deletion

sgRNA name	Target strand	PAM	Forward oligo (5'→3')	Reverse oligo (5'→3')
sgRNA 1	(−)	TGG	CACCGACTCTGTCAGGTCATTACCG	AAACCGGTAATGACCTGACAGAGTC
sgRNA 2	(−)	GGG	CACCGGATAACTTCGTAACCACCAG	AAACCTGGTGGTTACGAAGTTATCC

METTL3: Methyltransferase-like 3; CRISPR: Clustered regularly interspaced short palindromic repeats; Cas9: CRISPR-associated protein 9; sgRNA: Single-guide RNA; PAM: Protospacer adjacent motif; Oligo: Oligonucleotide

Table 2: Primer sequences used for gap-PCR-based verification of CRISPR/Cas9-mediated *METTL3* deletion

Primer Name	Orientation	Sequence (5′→3′)	Amplicon size (before cut)	Amplicon size (after cut)	Notes
Primer #Fw	Forward (F)	CAGCAGTTCCTGAATTAGCTACAGA	~5.5 kb	~500 bp	Upstream of sgRNA1
Primer #Rev	Reverse (R)	CAAGGGTGATCCTGAAACAGTGTA	~5.5 kb	~500 bp	Downstream of sgRNA2

Expected amplicon sizes before and after genome editing are indicated. gap-PCR: Gap-polymerase chain reaction; CRISPR: Clustered regularly interspaced short palindromic repeats; Cas9: CRISPR-associated protein 9; Fw: Forward; Rev: Reverse; sgRNA: Single-guide RNA; kb: Kilo base; bp: Base pair

Structural Modeling of Wild-Type and Truncated METTL3

To assess the structural consequences of the predicted genomic deletion, three-dimensional models of the wild-type and truncated METTL3 proteins were generated. The full-length METTL3 sequence was used to predict the wild-type structure, whereas the truncated sequence was used to predict the mutant structure. Structure prediction was performed using AlphaFold2 implemented through the ColabFold notebook (https://colabfold.com/) with default parameters. The resulting models were visualized and structurally compared using PyMOL (version 3.1.1) to assess the predicted structural loss of the catalytic methyltransferase domain (figure 2).

Cloning and Verification of sgRNAs

Two sgRNAs were independently cloned into the pSpCas9(BB)-2A-GFP (PX458) vector (plasmid #48138; Addgene, Watertown, MA, USA) using a standard single-step digestion–ligation workflow. The PX458 plasmid expresses SpCas9 and the sgRNA under cytomegalovirus (CMV) and U6 promoters and includes a green fluorescent protein (GFP) reporter for enrichment of transfected cells. The plasmid also carries an ampicillin resistance gene for bacterial selection.

Oligonucleotides encoding each sgRNA were annealed with their complementary strands and ligated into the PX458 vector digested with the BbsI restriction enzyme (Cat. No. ER1011, Thermo Fisher Scientific, USA) using T4 DNA ligase (Cat. No. EL0014, Thermo Fisher Scientific, USA). The resulting constructs were transformed into competent *Escherichia coli* DH5α cells and selected on LB agar plates (Sigma-Aldrich, USA) supplemented with ampicillin (Sigma-Aldrich, USA).

Putative positive colonies were screened by colony polymerase chain reaction (PCR) using a vector-specific forward primer together with the corresponding sgRNA oligonucleotide as the reverse primer. Three colonies for each sgRNA construct were randomly selected and analyzed. PCR amplification was initiated with a denaturation step at 95 °C for 5 min, followed by a touch-down cycling protocol in which the annealing temperature was gradually decreased from 68 °C to 55.4 °C at a rate of 0.8 °C per cycle across 17 cycles (95 °C for 30 s, 68–55.4 °C for 30 s, and 72 °C for 20 s). Subsequently, 20 additional cycles were performed using a constant annealing temperature of 55.4 °C, followed by a final extension at 72 °C for 7 min. PCR products were resolved on 2% agarose gels alongside a 100-bp DNA ladder (Catalogue Number: SL 7041, Sinaclon, Iran), and colonies showing the expected 141-bp band were expanded in liquid culture. Plasmid DNA was purified using a Miniprep Kit (Catalogue Number: FAPDE 050, Favorgen, Taiwan).

Purified plasmids from two independent positive colonies for each sgRNA construct were further analyzed by two PCR assays. First, amplification using the same primer combination employed for colony PCR reconfirmed sgRNA integration. Second, the sgRNA insertion region was amplified using paired vector-specific primers, including an in-house designed forward primer (5′-TTCTTGGGTAGTTTGCAGTTTTAA-3′) and reverse primer (5′-CACGCGCTA AAAACGGACTA-3′).[33] These primers were previously validated in our laboratory and were designed to flank the sgRNA insertion site within the vector, generating a 241-bp product encompassing the sgRNA sequence.

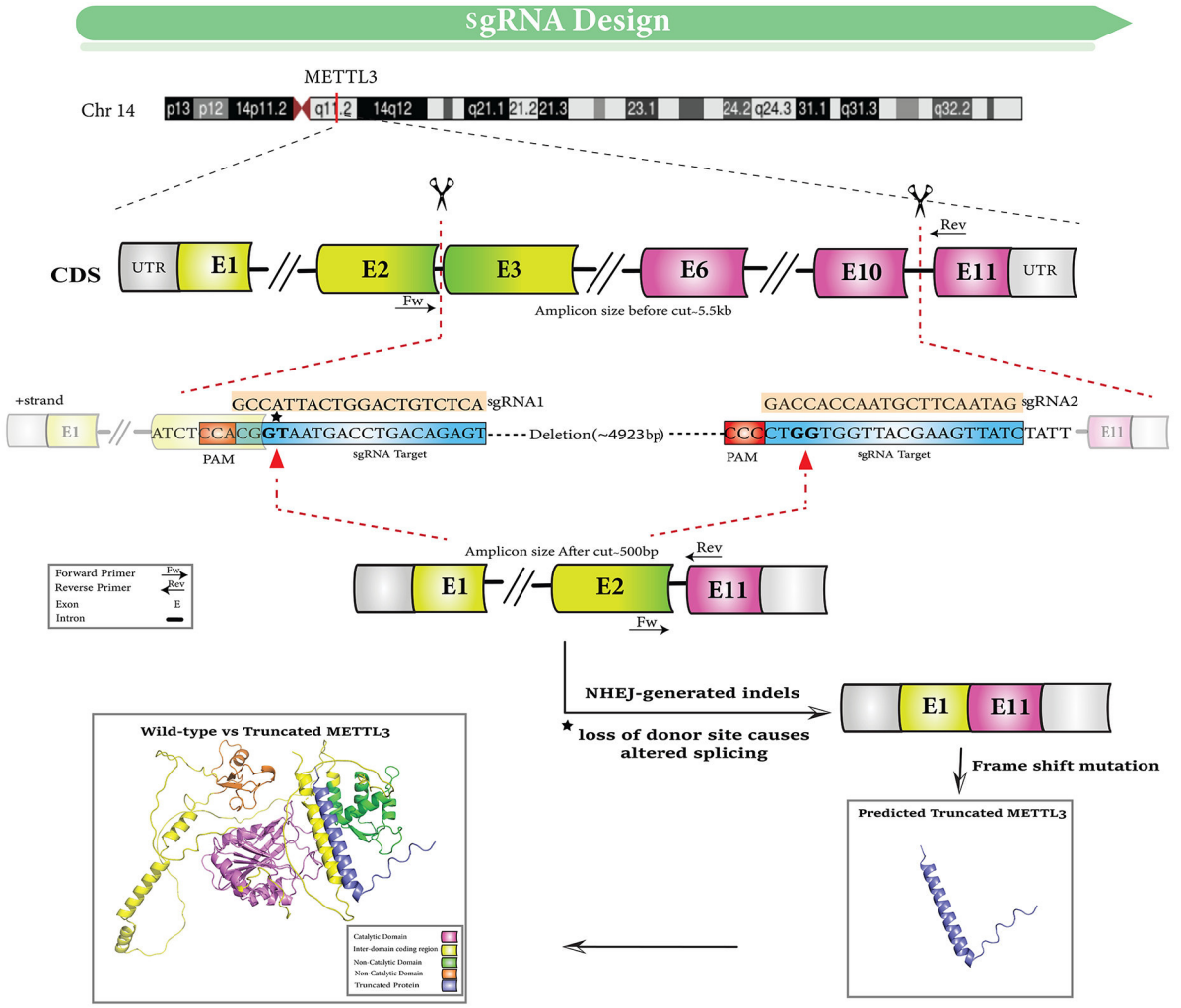


Figure 2: Dual-sgRNA CRISPR/Cas9 strategy used in this study to target *METTL3* is illustrated. Two sgRNAs were designed to target intron 2 and intron 10 of the *METTL3* gene, resulting in excision of exons 3–10 and predicted disruption of normal pre-mRNA splicing, potentially leading to a frameshift and predicted truncation of the METTL3 lacking the catalytic domain. Predicted structures of wild-type and truncated METTL3 were generated using AlphaFold2 via ColabFold and visualized with PyMOL (version 3.1.1). sgRNAs: Single guide RNA; CRISPR: Clustered regularly interspaced short palindromic repeats; Cas9: CRISPR-associated protein 9; *METTL3: Methyltransferase-like 3*; pre-mRNA: Precursor messenger RNA; Chr: Chromosome; UTR: Untranslated region; CDS: Coding sequence; E: Exon; Fw: Forward primer; Rev: Reverse primer; sgRNA: Single-guide RNA; PAM: Protospacer adjacent motif; NHEJ: Non-homologous end joining; bp: Base pair; kb: Kilo base

The amplified fragment was then used for Sanger sequencing to verify correct sgRNA insertion.

Cell Culture

In this study, the immortalized hepatoblastoma-derived cell line HepG2, exhibiting epithelial-like morphology, was obtained from the Pasteur Institute (Tehran, Iran). Cells were cultured at 37 °C in a humidified atmosphere containing 5% CO_2 using Dulbecco's Modified Eagle Medium/Nutrient Mixture F-12 (DMEM/F12; Catalogue Number: 11320033, Gibco, Iran), supplemented with 10% (v/v) fetal bovine serum (Catalogue Number: A5256701, Gibco, Iran), 100 U/mL penicillin, and 100 µg/mL streptomycin (Catalogue Number: XC-A4122/20, Biosera, France).

Transfection

At the fifth passage, HepG2 cells were trypsinized using 0.05% trypsin/EDTA (Catalogue Number: 25200056, Gibco, USA) upon reaching 60-70% confluency and seeded into six-well plates at a density of approximately 8.5×10^5 cells per well. After 24 hours of incubation, when cell confluency reached approximately 80%, cells were co-transfected with sgRNA1- and sgRNA2-containing CRISPR/Cas9 constructs using Lipofectamine 3000 (Catalogue Number: L3000008, ThermoFisher Scientific, USA). For each well, 1.25 µg of each sgRNA plasmid (2.5 µg total DNA) was diluted in 125 µL Opti-MEM (Catalogue Number: 31985062, Gibco, USA) and mixed with 5 µL P3000 reagent. Separately, 3.75 µL Lipofectamine 3000 was diluted in 125 µL Opti-MEM.

The two solutions were then combined, vortexed for 3 sec, and incubated at room temperature for 15 min to allow complex formation (DNA: Lipofectamine ratio≈1:1.5). The cells were then incubated for 48 hours.

Transfection experiments were independently repeated at least three times to ensure reproducibility, and representative results from one experiment with typical transfection efficiency are presented. Mock-transfected HepG2 cells (Lipofectamine 3000 reagent without plasmid DNA) were included as procedural controls to monitor potential cytotoxic effects of the transfection procedure and to control for non-specific amplification in downstream PCR analyses.

FACS–Based Enrichment and Pooled Expansion of Transfected HepG2 Cells

Transfection efficiency was initially evaluated by fluorescence microscopy at 24 and 48 hours post-transfection. Cells were enzymatically detached, collected, and resuspended in 1,500 µL phosphate-buffered saline (PBS; Catalogue Number: BI-1404-05, Bioidea, Iran). Since the PX458 plasmid co-expresses SpCas9 and enhanced green fluorescent protein (eGFP), transfected cells were identified and enriched based on GFP fluorescence using fluorescence-activated cell sorting (FACS) on a BD FACSAria III cell sorter (BD Biosciences, USA). Flow cytometry data were analyzed by sequentially gating for viable singlets (P1/P2), followed by the identification of GFP-positive cells (P3). In a representative sorting experiment, approximately 1.4×10^4 GFP-positive cells were collected as a pooled, non-clonal population. These cells were expanded in fresh complete growth medium supplemented with 20% fetal bovine serum (FBS) before genomic DNA isolation and gap-polymerase chain reaction (gap-PCR) analysis. FACS enrichment experiments were performed in three independent biological replicates, and representative flow cytometry plots from experiments with comparable enrichment profiles are presented.

Genomic DNA Isolation and Gap-PCR Analysis

Genomic DNA was extracted from the expanded, pooled GFP-positive cells, as well as from non-transfected and mock-transfected HepG2 cells (negative controls), using the Blood/Cultured Cell Genomic DNA Extraction Mini Kit (Catalogue Number: FATGK001, Favorgen, Taiwan), in accordance with the manufacturer's instructions.

To detect and evaluate the CRISPR/Cas9-mediated genomic deletion, a gap-PCR assay was performed using primers flanking the predicted junction of excision. Amplification was performed with a forward primer (5′-GGCTC CTTGGTCAACAGATAGA-3′) located in exon 2, upstream of the intron 2–targeting sgRNA, and a reverse primer (5′-AAATCACA CCCATCCACATTTT-3′) positioned in exon 10, downstream of the intron 10–targeting sgRNA.

Gap-PCR amplification was carried out using an initial denaturation step at 95 °C for 5 min, followed by 35 cycles of denaturation at 95 °C for 30 sec, annealing at 60 °C for 30 sec, and elongation at 70 °C for 30 sec. The reaction was completed with a final extension step at 72 °C for 8 min. Amplicons were subsequently resolved by electrophoretic separation on agarose gels alongside a 50 bp DNA ladder (Catalogue Number: SL7021, Sinaclon, Iran).

Genetic Validation by Sanger Sequencing and TIDE/CRISPID

Sanger sequencing was performed on gap-PCR amplicons spanning the predicted deletion junction to assess the presence of the expected CRISPR/Cas9-mediated genomic rearrangement within the *METTL3* locus. Bulk gap-PCR products derived from the pooled GFP-positive cell population were directly subjected to Sanger sequencing without prior gel purification or clonal isolation. Sequencing chromatograms obtained from edited and non-transfected control cells were analyzed using the tracking of indels by decomposition (TIDE) web tool (https://tide.nki.nl)[34] and CRISPR indel detector (CRISP-ID) software (https://crispid.gbiomed.kuleuven.be)[35] to characterize the spectrum of genome editing outcomes and to estimate overall editing efficiency.

Editing efficiency was estimated from Sanger sequencing chromatograms of pooled edited cells relative to non-transfected controls to distinguish CRISPR-induced indels from background signal. The TIDE analysis window was centered on the predicted Cas9 cleavage site with an indel size range of -10 to +10 bp and a significance threshold of $P<0.001$. The editing efficiency was calculated as the cumulative frequency of predicted insertion and deletion events. CRISPR-ID analysis was used to confirm the predominant indel patterns.

Results

Design of a Dual-sgRNA CRISPR/Cas9 Strategy for METTL3 Targeted Deletion

In this study, *METTL3* was selected as the target locus for CRISPR/Cas9-mediated genomic deletion.

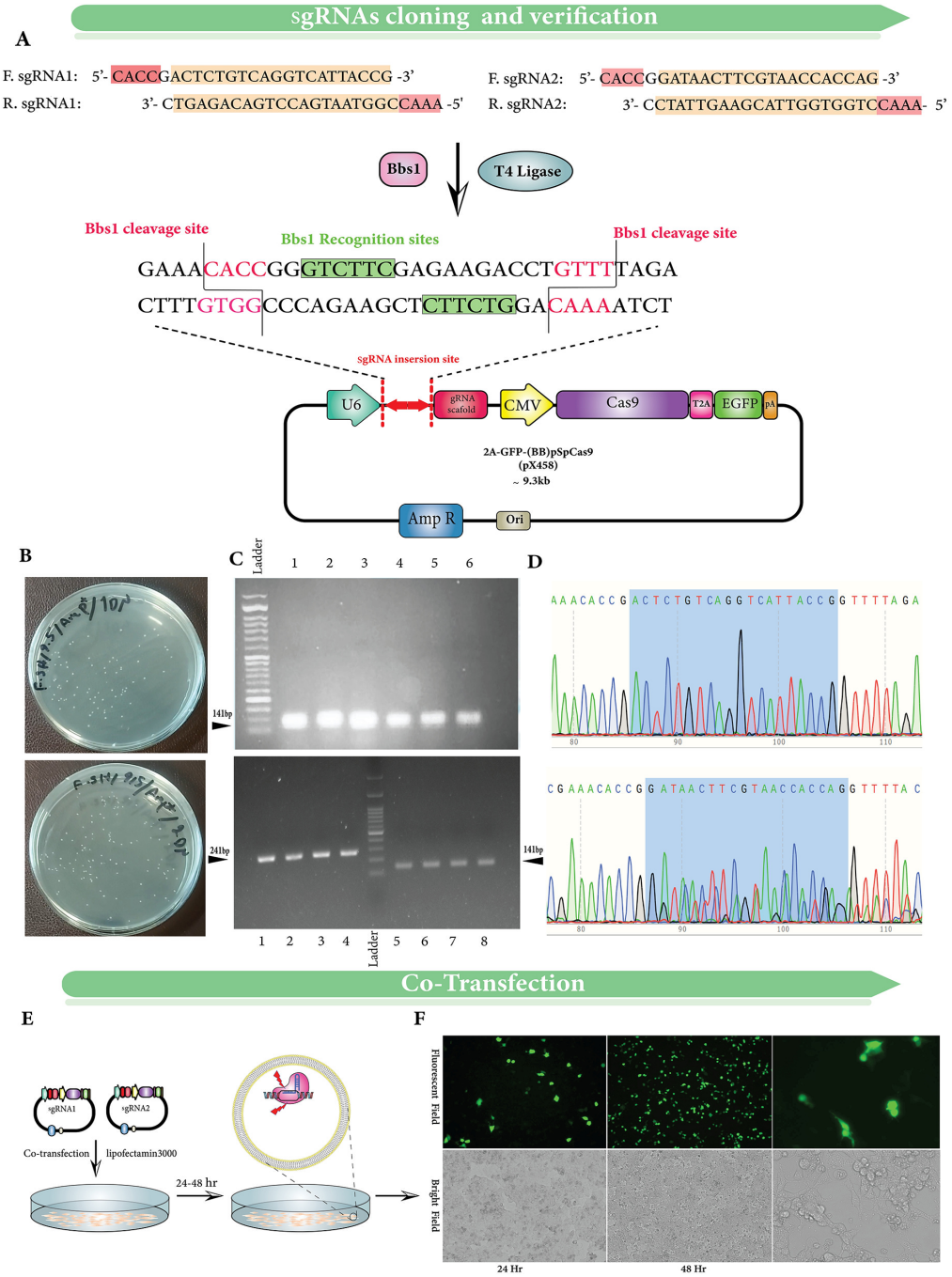


Figure 3: The sgRNA cloning strategy and transfection validation of *METTL3*-targeting CRISPR/Cas9 constructs are illustrated. (A) The insertion of *METTL3*-targeting sgRNAs into the BbsI-digested pX458 vector is schematically illustrated using T4 DNA ligase. (B) The figure shows the representative ampicillin-resistant colonies after transformation into *Escherichia coli* DH5α cells, with the top and bottom images corresponding to sgRNA1 and sgRNA2, respectively. (C) PCR validation of positive sgRNA clones is presented. In the upper panel (lanes 1–6), colony PCR demonstrates the expected 141-bp amplicon from three independent colonies for each sgRNA. The lower panel displays plasmid-based validation using two independent clones per sgRNA, where amplification with vector-specific primers flanking the insertion site generated the expected 241-bp product (lanes 1–4), while confirmation using a vector-specific forward primer paired with the corresponding sgRNA oligonucleotide as the reverse primer yielded the expected 141-bp amplicon (lanes 5–8). (D) Sanger sequencing chromatograms confirm the correct insertion and sequence integrity of both sgRNAs within the pX458 backbone. (E) A schematic overview of the dual-sgRNA co-transfection strategy in HepG2 cells is provided. (F) Representative enhanced green fluorescent protein (eGFP) fluorescence and bright-field images of HepG2 cells at 24 hours and 48 hours post-transfection demonstrate efficient plasmid delivery. These images were acquired at 4× (left and middle) and 20× (right) magnification, and approximately 40–50% of the cells were eGFP-positive at 48 hours. *METTL3:* Methyltransferase-like 3; CRISPR: Clustered regularly interspaced short palindromic repeats; Cas9: CRISPR-associated protein 9; sgRNA: Single-guide RNA; F. sgRNA: Forward. Single-guide RNA; R. sgRNA: Reverse. single-guide RNA; PAM: Protospacer adjacent motif; BbsI: Type II restriction enzyme; CMV: Cytomegalovirus promoter; T2A: Thosea asigna virus 2A self-cleaving peptide; EGFP: Enhanced green fluorescent protein; pA: Polyadenylation signal; AmpR: Ampicillin resistance gene; Ori: Origin of replication; kb: Kilo base; bp: Base pair; hr: hour

Two CRISPR/Cas9 sgRNAs were designed to target intronic regions flanking exons 2 and 10, specifically within intron 2 and intron 10, to excise the intervening genomic segment and thereby disrupt normal precursor messenger RNA (pre-mRNA) splicing (table 1).

This dual sgRNA strategy was predicted to promote exon 2 skipping and aberrant splicing, potentially leading to a frameshift mutation and truncation of the METTL3 protein lacking the catalytic domain (figure 2).

Cloning and Verification of METTL3-Targeting sgRNAs

To target the *METTL3* gene, two specific sgRNAs were designed against intron 2 and intron 10 and independently cloned into the pSpCas9(BB)-2A-GFP (PX458) vector (figure 3A). Following transformation into *Escherichia coli* DH5α, ampicillin-resistant transformants were successfully obtained (figure 3B).

Initial screening by colony PCR confirmed the presence of the sgRNA inserts in three independent positive clones for each sgRNA construct, each yielding the expected 141-bp amplicon (figure 3C, upper panel, lanes 1–6). To ensure the integrity of the recombinant plasmids before downstream applications, plasmid DNA purified from two independent positive clones for each sgRNA was further validated using two PCR strategies. Amplification with a vector-specific forward primer paired with the corresponding sgRNA-specific reverse primer reconfirmed successful guide insertion (figure 3C, lower panel, lanes 1–4), while PCR using flanking vector-specific primers generated the expected 241-bp fragments spanning the sgRNA cloning site (figure 3C, lower panel, lanes 5–8).

Finally, the accuracy of the insertion and the sequence of each sgRNA were confirmed by Sanger sequencing. These results confirmed the correct insertion and sequence integrity of the *METTL3*-targeting sgRNAs within the PX458 vector (figure 3D).

CRISPR/Cas9 Transfection Efficiency and FACS-Based Enrichment in HepG2 Cells

To induce a targeted deletion at the *METTL3* locus, HepG2 cells were co-transfected with dual-sgRNA CRISPR/Cas9 plasmids targeting intron 2 and intron 10. Transfection efficiency was monitored by GFP fluorescence microscopy. Across independent transfection experiments, GFP expression was consistently observed in approximately 40–50% of cells at 48 hours post-transfection, indicating efficient plasmid delivery (figure 3F). Images from a representative experiment are shown.

Subsequently, GFP-positive cells were enriched by FACS. This approach yielded a clearly defined singlet GFP-positive population, accounting for approximately 36.5% of the total gated cells (figure 4A). The FACS-enriched GFP-positive cells were then expanded as a pooled, non-clonal population for downstream genomic validation and molecular analyses (figure 4B).

Genomic Validation of METTL3 Deletion by Gap-PCR, Sanger Sequencing, and TIDE/CRISP-ID Analysis

To validate the CRISPR/Cas9-mediated genomic deletion of *METTL3*, total genomic DNA was isolated from the transfected HepG2 cell population, with non-transfected cells included as a negative control. Gap-PCR was performed using primer pairs flanking the predicted deletion region spanning exons 2-10. Electrophoretic analysis of the gap-PCR products revealed a distinct amplified fragment of approximately 500 bp exclusively in the transfected cells, consistent with the anticipated CRISPR/Cas9-induced excision. In contrast, no detectable PCR product was observed in non-transfected control cells, as amplification of the intact *METTL3* allele would generate a large fragment (~5.5 kb) that is inefficiently amplified under these conditions (figure 4C). Mock-transfected cells also produced no detectable gap-PCR product, further confirming that the observed amplification was specific to CRISPR/Cas9-mediated genomic editing.

To further assess the genomic alteration at nucleotide resolution, gap-PCR amplicons derived from edited cells were subjected to Sanger sequencing. The resulting chromatograms revealed a mixed pattern characterized by clear sequence alignment up to the predicted sgRNA1 cleavage site, followed by overlapping peaks consistent with the presence of a deletion junction and heterogeneous indel events at the targeted locus (figures 4D–E). Consistent with these findings, CRISP-ID analysis demonstrated a pronounced enrichment of indel events centered around the expected cleavage site, supporting on-target genome editing (figure 4E). Complementary TIDE analysis estimated an overall editing efficiency of approximately 34%, with deletion events representing the predominant editing outcome, while minor insertion and alternative deletion events were detected at lower frequencies (figure 4F).

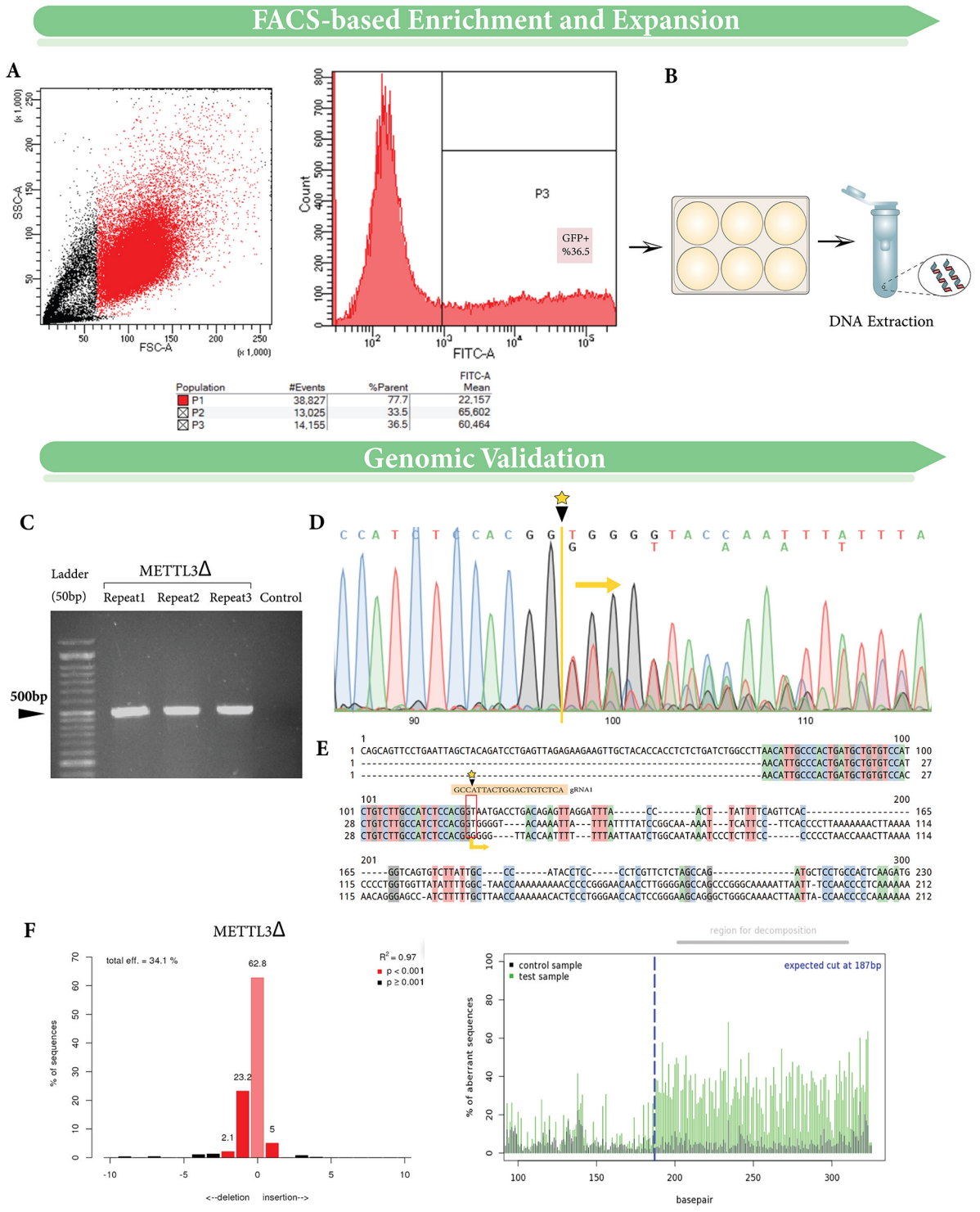


Figure 4: FACS-based enrichment and genomic validation of *METTL3* deletion in HepG2 cells are shown. (A) A flow cytometry-based gating strategy illustrates singlet discrimination and enrichment of GFP-positive HepG2 cells following co-transfection with dual-sgRNA CRISPR/Cas9 plasmids, yielding a singlet GFP-positive population of approximately 36.5%. (B) A schematic overview depicts pooled expansion of GFP-positive cells and subsequent genomic DNA extraction for downstream genome-editing validation and molecular analyses. (C) Gap-PCR analysis demonstrates an approximately 500-bp amplicon corresponding to the predicted large-scale genomic deletion at the *METTL3* locus. (D) Representative Sanger sequencing chromatograms reveal breakpoint junctions at the expected Cas9 cleavage sites. (E) Sequence alignment supported genomic excision at the *METTL3* target locus. (F) TIDE analysis estimated an overall genome-editing efficiency of approximately 34%. FACS: Fluorescence-activated cell sorting; *METTL3: Methyltransferase-like 3*; GFP: Green fluorescent protein; sgRNA: Single-guide RNA; CRISPR: Clustered regularly interspaced short palindromic repeats; Cas9: CRISPR-associated protein 9; PCR: Polymerase chain reaction; TIDE: Tracking of indels by decomposition; FSC-A: Forward scatter area; SSC-A: Side scatter area; FITC-A: Fluorescein isothiocyanate area; bp: Base pair. The black triangle marks the predicted *METTL3* deletion junction validated by gap-PCR and TIDE analysis. The yellow star indicates the predicted Cas9 cleavage site for sgRNA1.

Discussion

In the present study, we aimed to establish a dual-sgRNA CRISPR/Cas9 approach for the targeted deletion of the *METTL3* catalytic region in HepG2 cells. Our findings demonstrated the presence of a deletion-specific PCR product in the transfected cell population, while bulk Sanger sequencing and TIDE analysis provided supportive evidence of CRISPR-mediated editing in pooled GFP-positive cells. Together, these findings indicated that the designed strategy could generate targeted genomic alterations in HepG2 cells and might serve as a preliminary basis for future clonal and functional studies on METTL3 in MASLD.

m^{6}A-mediated epitranscriptomic regulation, primarily catalyzed by METTL3, plays an important role in hepatic metabolism and MASLD progression.[6, 8] However, evidence regarding the role of METTL3 in MASLD remains variable across different experimental contexts. Increased METTL3 activity has been associated with hepatic lipid accumulation and inflammatory signaling,[7] whereas hepatocyte-specific deletion has also been reported to aggravate steatosis and liver injury.[16] These divergent findings might reflect differences in disease stage, metabolic context, and the contributions of non-parenchymal liver cells, including Kupffer cells, hepatic stellate cells, and liver sinusoidal endothelial cells.[18, 36] Given this context-dependent complexity, the establishment of an effective genomic editing framework might facilitate investigation of the specific functions of METTL3 in hepatic cells.

Considering the challenges associated with incomplete METTL3 inactivation, including residual activity from alternatively spliced isoforms and the limitations of conventional knockdown and single-sgRNA CRISPR approaches,[24, 37] we designed a dual-sgRNA CRISPR/Cas9 strategy targeting the *METTL3* catalytic domain. Unlike single-sgRNA approaches, which rely primarily on stochastic indel formation within coding regions, this dual-sgRNA design targeted flanking intronic regions to excise the catalytic domain through a defined genomic deletion. This approach enables deletion-specific PCR-based assessment of the edited locus and reduces reliance on indel formation alone for functional disruption. Although indels may still occur at the repair junction, the designed excision is predicted to introduce a frameshift expected to disrupt the *METTL3* catalytic region, consistent with *in silico* structural modeling predictions.

Mechanistically, sgRNA1 was designed to target the 5′ region of intron 2 such that the canonical donor splice site overlaps the predicted Cas9 cleavage site. Disruption of this splice donor site may interfere with normal pre-mRNA splicing and potentially promote exon 2 skipping during transcript processing. Under this scenario, exon 1 may splice directly to exon 11, introducing a frameshift and likely generating a premature stop codon. Importantly, residues involved in *S*-adenosylmethionine (SAM) binding and methyltransferase activity begin in exon 6 and extend toward exon 11. Therefore, the predicted exon 1–11 junction would remove most of the catalytic region required for methyltransferase activity. Although these transcript and protein outcomes were not experimentally validated in the present study, the deletion strategy was designed to reduce the likelihood that splice-derived isoforms retaining catalytic activity would persist after genome editing.

Dual-sgRNA CRISPR strategies can enable defined multi-exon deletions and are designed to facilitate functional gene disruption. In this context, the edited HepG2 cell population generated here provides an initial experimental basis for subsequent transcriptomic, epitranscriptomic, and metabolic analyses relevant to MASLD. Following the establishment of stable edited cell lines, further studies, such as transcriptomic profiling, RNA methylation mapping, and metabolic assays, could help clarify the downstream molecular consequences of *METTL3* disruption. For example, lipid accumulation assays and gene expression analyses may help determine how METTL3-mediated m^{6}A modification influences hepatic lipid metabolism. In addition, this engineered system might be integrated into more complex multicellular liver models, including co-culture systems incorporating hepatocyte and hepatic stellate cell lines or three-dimensional hepatic spheroid models, to facilitate investigation of disease-relevant cellular interactions.[38-40]

Several limitations of the present study should be considered. First, the observed editing efficiency of approximately 34% reflected the heterogeneous nature of pooled CRISPR-edited cell populations. Although the presence of a deletion-specific PCR band indicated that the designed sgRNAs successfully induced targeted excision at the *METTL3* locus, the resulting population likely contained a mixture of edited and unedited alleles, as well as diverse repair outcomes. The absence of a wild-type PCR band might reflect inefficient amplification of the larger fragment, although this was not experimentally verified. Importantly, the ~500 bp amplicon

was not detected in non-transfected control cells, indicating that this fragment represents a deletion-specific junction generated following CRISPR editing.

Second, editing efficiency was estimated using bulk Sanger sequencing followed by TIDE analysis and therefore represented an approximation rather than an exact quantitative measurement. GFP-positive cells were enriched by fluorescence-activated cell sorting and subsequently expanded as a pooled population rather than isolated as individual clones. This strategy was selected as the primary objective of the present study was to determine whether the designed dual-sgRNA approach could generate the intended genomic deletion. However, pooled populations often contain heterogeneous editing outcomes, including partial deletions, indel variants, and unedited alleles. Consequently, molecular or phenotypic measurements derived from pooled populations might reflect averaged signals across genetically distinct subpopulations. Future clonal isolation and characterization will therefore be necessary to establish precise genotype–phenotype relationships. Additional variability might arise from DNA repair processes that generate heterogeneous junction sequences at the deletion site. Moreover, the HepG2 cell line does not fully reproduce the metabolic complexity of primary human hepatocytes.[41] Although HepG2 cells are widely used for studies of hepatic gene regulation, their metabolic properties differ from those of primary liver tissue. Accordingly, the system described here should be regarded as an initial experimental framework rather than a fully representative model of hepatic metabolic physiology.

Finally, several experimental validations remain to be addressed in future studies. Protein-level confirmation of *METTL3* disruption was not performed, and no functional or phenotypic assays were conducted. Therefore, the present findings support only the occurrence of genomic deletion at the *METTL3* locus. In addition, exon 2 skipping, the potential formation of an exon 1–11 splice junction, and the resulting frameshift mutation were predicted based on the deletion design and computational analyses. However, these predictions were not experimentally validated through transcript-level analyses, such as conventional RT-PCR targeting the predicted splice junction, splice-junction sequencing, or quantitative real-time PCR, or through protein-level assays, such as western blotting. Experimental evaluation of potential off-target effects was also not performed. The sgRNAs used in this study were selected using stringent computational criteria, including predicted cutting efficiency scores above 60, high MIT and CFD specificity scores, and the absence of predicted off-target sites within coding exons or seed regions. Furthermore, the guides were positioned to promote excision of the METTL3 catalytic domain through a large genomic deletion, thereby reducing the likelihood that intact coding sequences or potentially functional alternative isoforms would remain. Nevertheless, comprehensive experimental validation of off-target effects and molecular consequences of the engineered deletion will be required in future investigations.

Conclusion

In this study, we developed a dual-sgRNA CRISPR/Cas9 strategy targeting the *METTL3* locus in HepG2 cells and detected a deletion-specific PCR product consistent with excision of the catalytic region. Bulk Sanger sequencing and TIDE analysis further supported CRISPR-mediated editing within the pooled population, establishing a preliminary *in vitro* framework for studying m^{6}A-associated mechanisms in MASLD.

Future studies should include clonal isolation, transcript- and protein-level validation, off-target assessment, and downstream metabolic and phenotypic analyses. Following the generation of stable *METTL3*-disrupted cell lines and their integration with additional hepatic cell types, this platform might support investigation of m^{6}A-dependent regulation in MASLD using more physiologically relevant systems, including multicellular co-culture models and three-dimensional liver microtissues.

Acknowledgment

The authors would like to acknowledge the Transplant Research Center, Comprehensive Stem Cell Center, and Regenerative Medicine Institute, Shiraz University of Medical Sciences, for providing laboratory equipment and materials. We also thank the Department of Medical Genetics, Shiraz University of Medical Sciences, Shiraz, Iran, for hosting this research project and for their technical support. This study was extracted from the thesis of Faezeh Shafiei and was financially supported by Shahid Sadoughi University of Medical Sciences, Yazd, Iran (Grant no. 13593).

Authors' Contribution

F.S: Conceptualization; experimental and bioinformatic design; data curation and formal

analysis; figure preparation, drafting and editing; N.A: Conceptualization; supervision; resource provision; critical review and editing the manuscript; M.D: Methodology; validation; review and editing the manuscript; N.K: Methodology; validation; review and editing the manuscript; J.F: Methodology; validation; review and editing the manuscript; S.M.G.H: Methodology; review and editing the manuscript; M.L: Methodology; review and editing the manuscript; M.F.H: Methodology; review and editing the manuscript; A.D: Conceptualization; review and editing the manuscript; All authors have read and approved the final manuscript and agree to be accountable for all aspects of the work in ensuring that questions related to the accuracy or integrity of any part of the work are appropriately investigated and resolved.

Declaration of AI

During the preparation of this manuscript, the authors used ChatGPT-5.2 (OpenAI) solely for language editing, grammar improvement, and enhancement of clarity and readability. No artificial intelligence tools were used for data generation, analysis, interpretation, or figure preparation. All scientific content, results, and conclusions are the sole responsibility of the authors.

Conflict of Interest: None declared.

References

1 Xu B, Li H, Pi Y, Li K. Global, regional and national burden of Metabolic dysfunction-associated steatotic liver disease in adolescents and adults aged 15-49 years from 1990 to 2021: results from the 2021 Global Burden of Disease study. Front Med (Lausanne). 2025;12:1568211. doi: 10.3389/fmed.2025.1568211. PubMed PMID: 40636383; PubMed Central PMCID: PMC12237898.

2 Younossi ZM, Kalligeros M, Henry L. Epidemiology of metabolic dysfunction-associated steatotic liver disease. Clin Mol Hepatol. 2025;31:S32-S50. doi: 10.3350/cmh.2024.0431. PubMed PMID: 39159948; PubMed Central PMCID: PMC11925440.

3 Mejia-Guzman JE, Belmont-Hernandez RA, Chavez-Tapia NC, Uribe M, Nuno-Lambarri N. Metabolic-Dysfunction-Associated Steatotic Liver Disease: Molecular Mechanisms, Clinical Implications, and Emerging Therapeutic Strategies. Int J Mol Sci. 2025;26. doi: 10.3390/ijms26072959. PubMed PMID: 40243565; PubMed Central PMCID: PMC11988898.

4 Dua A, Kumari R, Singh M, Kumar R, Pradeep S, Ojesina AI, et al. Metabolic Dysfunction-Associated Steatotic Liver Disease (MASLD): the interplay of gut microbiome, insulin resistance, and diabetes. Front Med (Lausanne). 2025;12:1618275. doi: 10.3389/fmed.2025.1618275. PubMed PMID: 40893881; PubMed Central PMCID: PMC12392282.

5 Li Y, Yang P, Ye J, Xu Q, Wu J, Wang Y. Updated mechanisms of MASLD pathogenesis. Lipids Health Dis. 2024;23:117. doi: 10.1186/s12944-024-02108-x. PubMed PMID: 38649999; PubMed Central PMCID: PMC11034170.

6 Zaccara S, Ries RJ, Jaffrey SR. Reading, writing and erasing mRNA methylation. Nat Rev Mol Cell Biol. 2019;20:608-24. doi: 10.1038/s41580-019-0168-5. PubMed PMID: 31520073.

7 Yang Y, Cai J, Yang X, Wang K, Sun K, Yang Z, et al. Dysregulated m6A modification promotes lipogenesis and development of non-alcoholic fatty liver disease and hepatocellular carcinoma. Mol Ther. 2022;30:2342-53. doi: 10.1016/j.ymthe.2022.02.021. PubMed PMID: 35192934; PubMed Central PMCID: PMC9171149.

8 Zha X, Gao Z, Li M, Xia X, Mao Z, Wang S. Insight into the regulatory mechanism of m(6)A modification: From MAFLD to hepatocellular carcinoma. Biomed Pharmacother. 2024;177:116966. doi: 10.1016/j.biopha.2024.116966. PubMed PMID: 38906018.

9 Liu J, Yue Y, Han D, Wang X, Fu Y, Zhang L, et al. A METTL3-METTL14 complex mediates mammalian nuclear RNA N6-adenosine methylation. Nat Chem Biol. 2014;10:93-5. doi: 10.1038/nchembio.1432. PubMed PMID: 24316715; PubMed Central PMCID: PMC3911877.

10 Cheng W, Li M, Zhang L, Zhou C, Yu S, Peng X, et al. New roles of N6-methyladenosine methylation system regulating the occurrence of non-alcoholic fatty liver disease with N6-methyladenosine-modified MYC. Front Pharmacol. 2022;13:973116. doi: 10.3389/fphar.2022.973116. PubMed PMID: 36120320; PubMed Central PMCID: PMC9471244.

11 Li Q, Xiang J. METTL3 promotes the progression of non-alcoholic fatty liver disease by mediating m6A methylation of FAS. Sci Rep. 2025;15:6162. doi: 10.1038/s41598-025-90419-z. PubMed PMID: 39979577;

PubMed Central PMCID: PMC11842791.
12 Li Y, Zhang Q, Cui G, Zhao F, Tian X, Sun BF, et al. m(6)A Regulates Liver Metabolic Disorders and Hepatogenous Diabetes. Genomics Proteomics Bioinformatics. 2020;18:371-83. doi: 10.1016/j.gpb.2020.06.003. PubMed PMID: 33160098; PubMed Central PMCID: PMC8242261.
13 Xie W, Ma LL, Xu YQ, Wang BH, Li SM. METTL3 inhibits hepatic insulin sensitivity via N6-methyladenosine modification of Fasn mRNA and promoting fatty acid metabolism. Biochem Biophys Res Commun. 2019;518:120-6. doi: 10.1016/j.bbrc.2019.08.018. PubMed PMID: 31405565.
14 Li Y, Zhang D, Gao Y, Wang P, Wang Z, Zhang B, et al. METTL3 exacerbates insulin resistance in hepatocytes by regulating m(6)A modification of cytochrome P450 2B6. Nutr Metab (Lond). 2023;20:40. doi: 10.1186/s12986-023-00762-z. PubMed PMID: 37710320; PubMed Central PMCID: PMC10502999.
15 Peng Z, Gong Y, Wang X, He W, Wu L, Zhang L, et al. METTL3-m(6)A-Rubicon axis inhibits autophagy in nonalcoholic fatty liver disease. Mol Ther. 2022;30:932-46. doi: 10.1016/j.ymthe.2021.09.016. PubMed PMID: 34547464; PubMed Central PMCID: PMC8821937.
16 Li X, Yuan B, Lu M, Wang Y, Ding N, Liu C, et al. The methyltransferase METTL3 negatively regulates nonalcoholic steatohepatitis (NASH) progression. Nat Commun. 2021;12:7213. doi: 10.1038/s41467-021-27539-3. PubMed PMID: 34893641; PubMed Central PMCID: PMC8664922.
17 Dai G, Huang S, Li Y, Tu X, Xia J, Zhou Z, et al. Mettl3-mediated m(6)A modification plays a role in lipid metabolism disorders and progressive liver damage in mice by regulating lipid metabolism-related gene expression. Aging (Albany NY). 2023;15:5550-68. doi: 10.18632/aging.204810. PubMed PMID: 37335109; PubMed Central PMCID: PMC10333091.
18 Liao X, Liu L, Du J, Fan H, Yu Y, Luo Y, et al. METTL3 inhibits liver fibrosis via RBX1 stability and TXNIP-mediated ferroptosis. Hepatol Commun. 2025;9. doi: 10.1097/HC9.0000000000000752. PubMed PMID: 40658786; PubMed Central PMCID: PMC12263036.
19 Pan XY, Bi YH, Cheng M, Qian ZZ, Wang L, You HM, et al. METTL3 facilitates hepatic fibrosis progression via m6A-YTHDF2-dependent silencing of GPR161. bioRxiv. 2021:2021.12.15.472749. doi: 10.1101/2021.12.15.472749.
20 Qin Y, Li B, Arumugam S, Lu Q, Mankash SM, Li J, et al. m(6)A mRNA methylation-directed myeloid cell activation controls progression of NAFLD and obesity. Cell Rep. 2021;37:109968. doi: 10.1016/j.celrep.2021.109968. PubMed PMID: 34758326; PubMed Central PMCID: PMC8667589.
21 Cui B, Tu S, Li H, Zeng Z, Xiao R, Guo J, et al. METTL3 knockout accelerates hepatocarcinogenesis via inhibiting endoplasmic reticulum stress response. FEBS Open Bio. 2025;15:1144-58. doi: 10.1002/2211-5463.70023. PubMed PMID: 40103332; PubMed Central PMCID: PMC12226423.
22 Pan Y, Chen H, Zhang X, Liu W, Ding Y, Huang D, et al. METTL3 drives NAFLD-related hepatocellular carcinoma and is a therapeutic target for boosting immunotherapy. Cell Rep Med. 2023;4:101144. doi: 10.1016/j.xcrm.2023.101144. PubMed PMID: 37586322; PubMed Central PMCID: PMC10439254.
23 Poh HX, Mirza AH, Pickering BF, Jaffrey SR. Alternative splicing of METTL3 explains apparently METTL3-independent m6A modifications in mRNA. PLoS Biol. 2022;20:e3001683. doi: 10.1371/journal.pbio.3001683. PubMed PMID: 35853000; PubMed Central PMCID: PMC9295969.
24 Smith I, Greenside PG, Natoli T, Lahr DL, Wadden D, Tirosh I, et al. Evaluation of RNAi and CRISPR technologies by large-scale gene expression profiling in the Connectivity Map. PLoS Biol. 2017;15:e2003213. doi: 10.1371/journal.pbio.2003213. PubMed PMID: 29190685; PubMed Central PMCID: PMC5726721.
25 Goel K, Ploski JE. RISC-y Business: Limitations of Short Hairpin RNA-Mediated Gene Silencing in the Brain and a Discussion of CRISPR/Cas-Based Alternatives. Front Mol Neurosci. 2022;15:914430. doi: 10.3389/fnmol.2022.914430. PubMed PMID: 35959108; PubMed Central PMCID: PMC9362770.
26 Li H, Yang Y, Hong W, Huang M, Wu M, Zhao X. Applications of genome editing technology in the targeted therapy of human diseases: mechanisms, advances and prospects. Signal Transduct Target Ther. 2020;5:1. doi: 10.1038/s41392-019-0089-y. PubMed PMID: 32296011; PubMed Central PMCID: PMC6946647.
27 Tuladhar R, Yeu Y, Tyler Piazza J, Tan Z, Rene Clemenceau J, Wu X, et al. CRISPR-Cas9-based mutagenesis frequently

provokes on-target mRNA misregulation. Nat Commun. 2019;10:4056. doi: 10.1038/s41467-019-12028-5. PubMed PMID: 31492834; PubMed Central PMCID: PMC6731291.
28 Smits AH, Ziebell F, Joberty G, Zinn N, Mueller WF, Clauder-Munster S, et al. Biological plasticity rescues target activity in CRISPR knock outs. Nat Methods. 2019;16:1087-93. doi: 10.1038/s41592-019-0614-5. PubMed PMID: 31659326.
29 Fazelzadeh Haghighi M, Jafari Khamirani H, Fallahi J, Monfared AA, Ashrafi Dehkordi K, Tabei SMB. Novel insight into FCSK-congenital disorder of glycosylation through a CRISPR-generated cell model. Mol Genet Genomic Med. 2024;12:e2445. doi: 10.1002/mgg3.2445. PubMed PMID: 38722107; PubMed Central PMCID: PMC11080630.
30 Concordet JP, Haeussler M. CRISPOR: intuitive guide selection for CRISPR/Cas9 genome editing experiments and screens. Nucleic Acids Res. 2018;46:W242-W5. doi: 10.1093/nar/gky354. PubMed PMID: 29762716; PubMed Central PMCID: PMC6030908.
31 Bae S, Park J, Kim JS. Cas-OFFinder: a fast and versatile algorithm that searches for potential off-target sites of Cas9 RNA-guided endonucleases. Bioinformatics. 2014;30:1473-5. doi: 10.1093/bioinformatics/btu048. PubMed PMID: 24463181; PubMed Central PMCID: PMC4016707.
32 Montague TG, Cruz JM, Gagnon JA, Church GM, Valen E. CHOPCHOP: a CRISPR/Cas9 and TALEN web tool for genome editing. Nucleic Acids Res. 2014;42:W401-7. doi: 10.1093/nar/gku410. PubMed PMID: 24861617; PubMed Central PMCID: PMC4086086.
33 Dara M, Razban V, Talebzadeh M, Moradi S, Dianatpour M. Using CRISPR/Cas9 System to Knock out Exon 48 in DMD Gene. Avicenna J Med Biotechnol. 2021;13:54-7. doi: 10.18502/ajmb.v13i2.5517. PubMed PMID: 34012519; PubMed Central PMCID: PMC8112140.
34 Brinkman EK, Chen T, Amendola M, van Steensel B. Easy quantitative assessment of genome editing by sequence trace decomposition. Nucleic Acids Res. 2014;42:e168. doi: 10.1093/nar/gku936. PubMed PMID: 25300484; PubMed Central PMCID: PMC4267669.
35 Dehairs J, Talebi A, Cherifi Y, Swinnen JV. CRISP-ID: decoding CRISPR mediated indels by Sanger sequencing. Sci Rep. 2016;6:28973. doi: 10.1038/srep28973. PubMed PMID: 27363488; PubMed Central PMCID: PMC4929496.
36 Wang X, Zhang L, Dong B. Molecular mechanisms in MASLD/MASH-related HCC. Hepatology. 2025;82:1303-24. doi: 10.1097/HEP.0000000000000786. PubMed PMID: 38349726; PubMed Central PMCID: PMC11323288.
37 Piao X, Meng D, Zhang X, Song Q, Lv H, Jia Y. Dual-gRNA approach with limited off-target effect corrects C9ORF72 repeat expansion in vivo. Sci Rep. 2022;12:5672. doi: 10.1038/s41598-022-07746-8. PubMed PMID: 35383205; PubMed Central PMCID: PMC8983752.
38 Haaker MW, Chang JC, Chung BK, Pieper TS, Noe F, Wang T, et al. Cellular Crosstalk Promotes Hepatic Progenitor Cell Proliferation and Stellate Cell Activation in 3D Co-culture. Cell Mol Gastroenterol Hepatol. 2025;19:101472. doi: 10.1016/j.jcmgh.2025.101472. PubMed PMID: 39892785; PubMed Central PMCID: PMC11968293.
39 Messner S, Fredriksson L, Lauschke VM, Roessger K, Escher C, Bober M, et al. Transcriptomic, Proteomic, and Functional Long-Term Characterization of Multicellular Three-Dimensional Human Liver Microtissues. Appl In Vitro Toxicol. 2018;4:1-12. doi: 10.1089/aivt.2017.0022. PubMed PMID: 32953943; PubMed Central PMCID: PMC7500040.
40 Sani F, Soufi Zomorrod M, Azarpira N, Soleimani M. The Effect of Mesenchymal Stem Cell-Derived Exosomes and miR17-5p Inhibitor on Multicellular Liver Fibrosis Microtissues. Stem Cells Int. 2023;2023:8836452. doi: 10.1155/2023/8836452. PubMed PMID: 37576406; PubMed Central PMCID: PMC10421706.
41 Ardisasmita AI, Schene IF, Joore IP, Kok G, Hendriks D, Artegiani B, et al. A comprehensive transcriptomic comparison of hepatocyte model systems improves selection of models for experimental use. Commun Biol. 2022;5:1094. doi: 10.1038/s42003-022-04046-9. PubMed PMID: 36241695; PubMed Central PMCID: PMC9568534.